Rare Metal Materials and Engineering
Volume 52, Issue 3, March 2023
Available online at www.rmme.ac.cn

Science Press

Cite this article as: Lu Yupeng, Meng Lingjian, Yin Hongliang, et al. Constitutive Models for Tensile Deformation Behavior of Ti-22Al-25Nb Alloy Sheet at Elevated Temperatures[J]. Rare Metal Materials and Engineering, 2023, 52(03): 785-790.

ARTICLE

Constitutive Models for Tensile Deformation Behavior of Ti-22Al-25Nb Alloy Sheet at Elevated Temperatures

Lu Yupeng[1], Meng Lingjian[1], Yin Hongliang[1], Lin Peng[1,2]

[1] College of Materials Science and Engineering, Taiyuan University of Technology, Taiyuan 030024, China; [2] National Key Laboratory of Science and Technology on Precision Heat Processing of Metals, Harbin Institute of Technology, Harbin 150001, China

Abstract: Isothermal uniaxial tension tests for O phase-based Ti-22Al-25Nb alloys were conducted at 1203–1283 K with temperature interval of 20 K. The strain rates were 2.5×10^{-4}, 5.0×10^{-4}, 1×10^{-3}, 2×10^{-3}, 4×10^{-3}, 1×10^{-2}, and 5×10^{-2} s^{-1}. The microstructures of specimens at different deformation temperatures were characterized. Through the experiment results, the material constants for the constitutive models are determined and the tensile deformation activation energies are 845 165 and 412 779 J/mol at α_2+B2/β+O three-phase region (1203 – 1243 K) and α_2+B2 two-phase region (1243 – 1283 K), respectively. Arrhenius-type constitutive models are constructed to characterize the tensile deformation behavior of Ti-22Al-25Nb alloy at different temperatures.

Key words: Ti_2AlNb; constitutive model; microstructure; deformation behavior

Conventional Ti_3Al-based titanium alloys have excellent mechanical properties at room temperatures. With the Nb addition, their tension strength and ductility at room temperature can be further enhanced. Banerjee[1] and Nandy[2] et al found the new ordered orthorhombic phase, namely O phase (Ti_2AlNb). Song et al[3] improved the plasticity of Ti_2AlNb alloys by high density electropulsing and investigated the enhancement mechanism. Yang et al[4] investigated the creep deformation mechanism and environmental effects of Ti_2AlNb alloys and proposed different creep deformation mechanisms. Boehlert[5–6] and Cowen[7] et al discussed the fabrication process (forging, rolling) and mechanical behavior (creep behavior, tensile behavior) of Ti_2AlNb alloys. Zhang et al[8] studied the tensile behavior and deformation mechanism of Ti-22Al-25Nb alloy with lamellar O phases. Sim et al[9] investigated the influence of mechanical alloying on the mechanical properties and microstructure of Ti_2AlNb alloys prepared by powder metallurgy and mechanical alloying (MA) coupled with spark plasma sintering (SPS).

Typical Ti_2AlNb alloys with the composition of Ti-22Al-25Nb (at%) exhibit the advantages of low density, fine creep resistance, and high specific strength and toughness at elevated temperatures[10–13], therefore attracting much attention as a lightweight structural material in aerospace and automotive industries[14–16]. However, the deformation behavior of Ti-22Al-25Nb titanium alloys at elevated temperatures has rarely been investigated. Generally, the constitutive equation is critical for the formability evaluation of alloys[17–22]. Richardson et al[23] proposed a model for the prediction of strain-stress relationship at elevated temperatures[18,24]. In addition, the microstructural evolution and phase transformation of Ti_2AlNb alloys at different temperatures are different, which affects the mechanical properties. Therefore, it is necessary to study the microstructural evolution of the alloy during deformation.

In this research, the deformation behavior of Ti_2AlNb alloys was studied through tension tests at different strain rates and temperatures. Moreover, the constitutive models of Ti-22Al-25Nb alloys at elevated temperatures and different strain rates were established. Finally, the effect of temperature on deformation activation energy was discussed based on the microstructure evolution.

1 Experiment

The as-received material used in this research was a hot-

Received date: September 20, 2022
Foundation item: National Natural Science Foundation of China (51505323); Applied Basic Research Program of Shanxi Province (20210302123117, 20210302124658)
Corresponding author: Lin Peng, Ph. D., Professor, College of Materials Science and Engineering, Taiyuan University of Technology, Taiyuan 030024, P. R. China, Tel: 0086-351-6010021, E-mail: linpeng@tyut.edu.cn

rolled Ti-22Al-25Nb alloy sheet with thickness of 1.25 mm, which contained 10.90wt% Al, 42.0wt% Nb, 0.07wt% O, 0.008wt% C, 0.006wt% N, and balance Ti. The raw sheets were heat-treated under different conditions: (1) at 1203, 1223, and 1243 K for 4 h; (2) at 1263 K for 2 h; (3) at 1283 K for 0.5 h. The final pass of hot-rolling for all heat-treated alloy sheets was conducted at 1213 K. The sheets were cooled down to room temperature by water spraying after the heat treatments. The uniaxial tensile specimens with gauge length of 10 mm and width of 3 mm were machined from the quenched sheet along the rolling direction by the low-speed electrical discharge machine.

The isothermal uniaxial tension tests were conducted by Instron 5500R electronic universal testing machine at 1203–1283 K with temperature interval of 20 K to investigate the influences of temperature and strain rate on the deformation behavior of Ti-22Al-25Ni alloys. The initial strain rates were 2.5×10^{-4}, 5.0×10^{-4}, 1×10^{-3}, 2×10^{-3}, 4×10^{-3}, 1×10^{-2}, and 5×10^{-2} s^{-1}. Thermal couples were installed in the heating furnace to measure the specimen temperature. Before isothermal uniaxial tension tests, the specimens were heated to the designed temperature and held for 300 s to eliminate the thermal gradient. Then, the specimens were stretched until fracture. True stress-true strain curves were recorded automatically by the Instron Bluehill software during the isothermal uniaxial tension tests.

To observe the microstructure of specimens at different deformation temperatures, the specimens were rapidly quenched in water after deformation. The deformed specimens were sectioned parallel to the tension axis. A Quanta 200 FEG scanning electron microscope (SEM) was used to observe the microstructure of the as-received and deformed specimens for investigation of the deformation mechanism and the influence of microstructure on the deformation activation energy.

2 Results and Discussion

2.1 Initial microstructure

Fig. 1 shows SEM microstructure of the as-received Ti-22Al-25Nb alloy. It is found that the dark, gray, and bright regions represent the α_2, O, and B2/β phases, respectively. The matrix microstructure consists of fine B2/β and lamellar O grains, and the equiaxed α_2 grains wrapped by rim-O grains are uniformly distributed in the matrix.

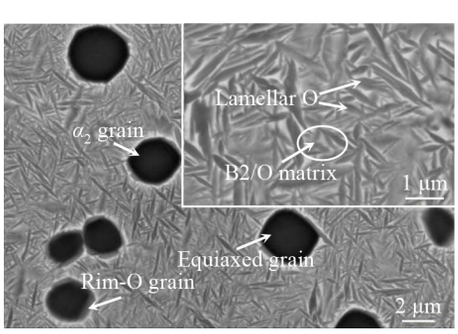

Fig.1 SEM microstructure of as-received Ti-22Al-25Nb alloy

2.2 Flow behavior

Fig. 2 shows the true stress-true strain curves of Ti-22Al-25Nb alloys during isothermal uniaxial tension tests. The four-section analytical method is used to discuss the deformation behavior[25]. In the first section, the true stress rises rapidly until the true strain reaches 0.05. This process is independent of strain rate and deformation temperature. The fast increase in stress can be attributed to the dramatically multiplied dislocations as well as the formation and multiplication of subgrain boundaries[26]. Moreover, with decreasing the temperature and increasing the strain rate, the peak stress becomes less distinct and the flow stress is increased significantly. In the second section, the softening phenomenon of the specimen occurs, where the true stress drops due to the initiation of homogeneous plastic deformation. The true stress drops slightly and the softening occurs more obviously at higher temperatures and lower strain rates due to the dynamic balance between the work hardening and dynamic softening[27]. Then, in the third section, the true stress drops sharply because of the localized necking. In the last section, the specimens fracture.

2.3 Constitutive equation

Constitutive equations are designed to depict the deformation behavior of alloy specimens at different temperatures. Parameter Z is used to express the relationship between the strain rate $\dot{\varepsilon}$ and temperature T[23,28], as follows:

$$Z = \dot{\varepsilon}\exp(Q/RT) \quad (1)$$

where Z is the Zener-Hollomon parameter, $\dot{\varepsilon}$ is the strain rate (s^{-1}), Q is the hot deformation activation energy ($J\cdot mol^{-1}$), R is

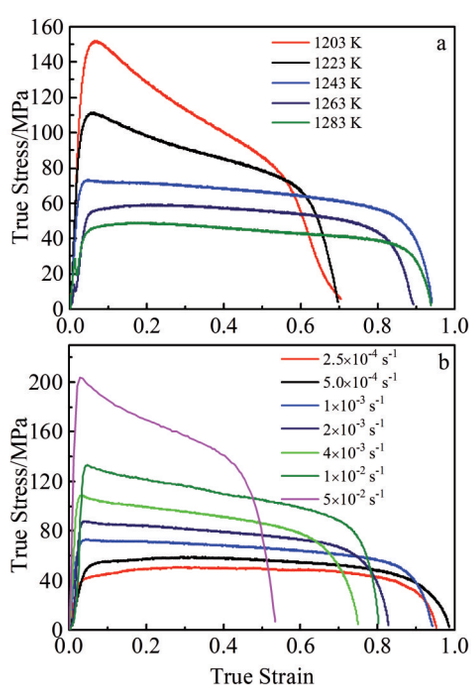

Fig.2 True stress-strain curves of Ti-22Al-25Nb alloys during isothermal uniaxial tension tests under different conditions: (a) at strain rate of 1×10^{-3} s^{-1} with different temperatures; (b) at 1243 K with different strain rates

the mole gas constant (8.3145 J·mol^{-1}·K^{-1}), and T is the absolute forming temperature (K).

The Arrhenius equation can accurately depict the relationship between the parameter Z and peak stress σ_p:

$$Z = F(\sigma_p) = A_1\sigma_p^{n_1} \quad \alpha\sigma_p<0.8 \tag{2}$$

$$Z = F(\sigma_p) = A_2\exp(\beta\sigma_p) \quad \alpha\sigma_p>1.2 \tag{3}$$

$$Z = F(\sigma_p) = A[\sinh(\alpha\sigma_p)]^n \quad \text{for all } \sigma_p \tag{4}$$

where A_1, A_2, A_3, n_1, n, α, and β are material constants.

By substituting Eq. (1) into Eq. (2 – 4), Eq. (5 – 7) can be obtained, respectively, as follows:

$$\dot{\varepsilon} = A_1\sigma_p^{n_1}\exp(-Q/RT) \tag{5}$$

$$\dot{\varepsilon} = A_2\exp(\beta\sigma_p)\exp(-Q/RT) \tag{6}$$

$$\dot{\varepsilon} = A[\sinh(\alpha\sigma_p)]^n\exp(-Q/RT) \tag{7}$$

In order to calculate the value of n_1 and β, Eq. (5 – 6) are transformed into Eq.(8–9), respectively, as follows:

$$\ln\sigma_p = \frac{1}{n_1}\ln\dot{\varepsilon} - \frac{1}{n_1}\ln A_1 + Q/RT \tag{8}$$

$$\sigma_p = \frac{1}{\beta}\ln\dot{\varepsilon} - \frac{1}{\beta}\ln A_2 + Q/\beta RT \tag{9}$$

The relationship between $\ln\sigma_p$ and $\ln\dot{\varepsilon}$ can be obtained, as shown in Fig. 3a. Through the linear regression method, the value of $1/n_1$ can be calculated from the slope of $\ln\sigma_p$-$\ln\dot{\varepsilon}$ line. Thus, n_1=3.785. Similarly, the value of $1/\beta$ can be calculated from the slope of σ_p-$\ln\dot{\varepsilon}$ line, as shown in Fig. 3b. Thus, β= 0.035 091 and $\alpha=\beta/n_1$=0.009 271 1.

In order to get the value of n, the logarithm form of Eq. (7) is used, as follows:

$$\ln\dot{\varepsilon}=\ln A+n\ln[\sinh(\alpha\sigma_p)]-Q/RT \tag{10}$$

The relationship between $\ln\dot{\varepsilon}$ and $\ln[\sinh(\alpha\sigma_p)]$ can be obtained, as shown in Fig. 3c. The fitting line slope in Fig. 3c represents the calculated value of n. As a result, the stress exponent of n is about 2.820 95.

Based on Eq.(10), Q can be obtained, as follows:

$$Q=nR\left\{\frac{\partial\ln[\sinh(\alpha\sigma_p)]}{\partial(1/T)}\right\}_{\dot{\varepsilon}} \tag{11}$$

The value of $\partial\ln[\sinh(\alpha\sigma_p)]/\partial(1000/T)$ can be evaluated by the fitting line slope, as shown in Fig. 3d, which is 36.036 at 1203 – 1243 K and 17.600 at 1243 – 1283 K. A great difference occurs due to the temperature range. Then, according to Eq. (11), the accurate value of Q at different temperatures can be obtained. It is calculated that Q=845 165 J/mol at 1203 – 1243 K, while Q =412 779 J/mol at 1243 – 1283 K.

In order to get the accurate value of Z, the logarithm form of Eq.(4) is used, as follows:

$$\ln Z=\ln A+n\ln[\sinh(\alpha\sigma_p)] \tag{12}$$

Combining Eq. (7), Eq. (13) can be obtained, as follows:

$$\dot{\varepsilon} = Z\exp(-Q/RT) \tag{13}$$

Therefore, the value of Z at different strain rates and different temperatures is determined.

By calculating, n and A are 2.570 and 8.377×10^{32} at 1203 – 1243 K, and 3.112 and 5.834×10^{14} at 1243 – 1283 K, respectively (Fig.3e).

According to the above discussion, the constitutive models of Ti-22Al-25Ti alloy are as follows:

$$\dot{\varepsilon} = 8.377\times10^{32}[\sinh(0.009\,271\,1\sigma_p)]^{2.570} \times\exp(-845\,165/RT) \quad T=1203–1243\ \text{K} \tag{14}$$

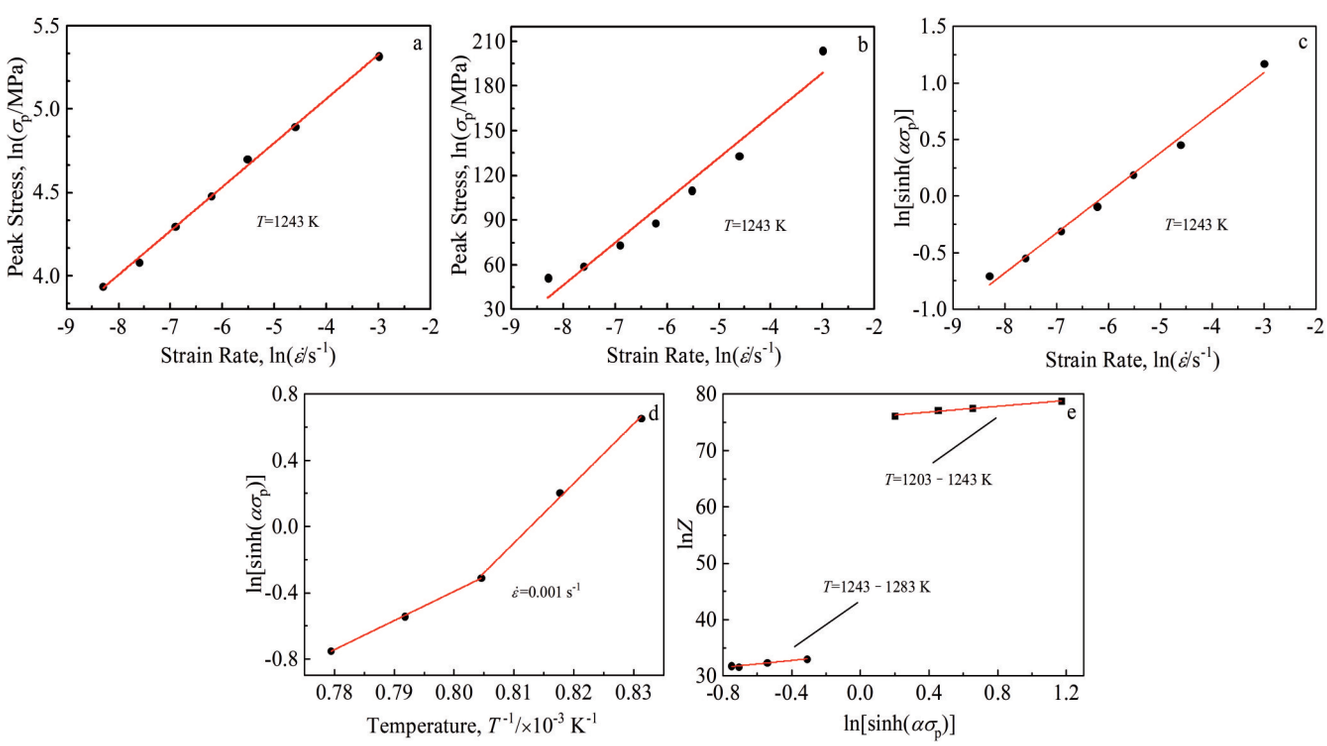

Fig.3 Relationships of $\ln\sigma_p$-$\ln\dot{\varepsilon}$ (a), σ_p-$\ln\dot{\varepsilon}$ (b), $\ln[\sinh(\alpha\sigma_p)]$-$\ln\dot{\varepsilon}$ (c), $\ln[\sinh(\alpha\sigma_p)]$-$T^{-1}$ (d), and $\ln Z$-$\ln[\sinh(\alpha\sigma_p)]$ (e)

$$\dot{\varepsilon} = 5.834 \times 10^{14}[\sinh(0.009\,271\,1\sigma_p)]^{3.112} \times \exp(-412\,779/RT) \quad T = 1243\text{–}1283\ K \tag{15}$$

2.4 Microstructure evolution

Fig. 4 shows SEM microstructures of the tensile specimens before and after tension at different temperatures with strain rate of 1×10^{-3} s^{-1}. It can be seen from Fig. 4a_1 that the alloy microstructure comprises α_2, B2, and lamellar O phases at 1203 K. The equiaxed α_2 grains are elongated during the hot deformation, indicating that the α_2 grains suffer a large plastic deformation at elevated temperature. The volume fraction of O phase is decreased with increasing the forming temperature. Fig. 4a_2 and 4b_2 show that the microstructure of O phase is

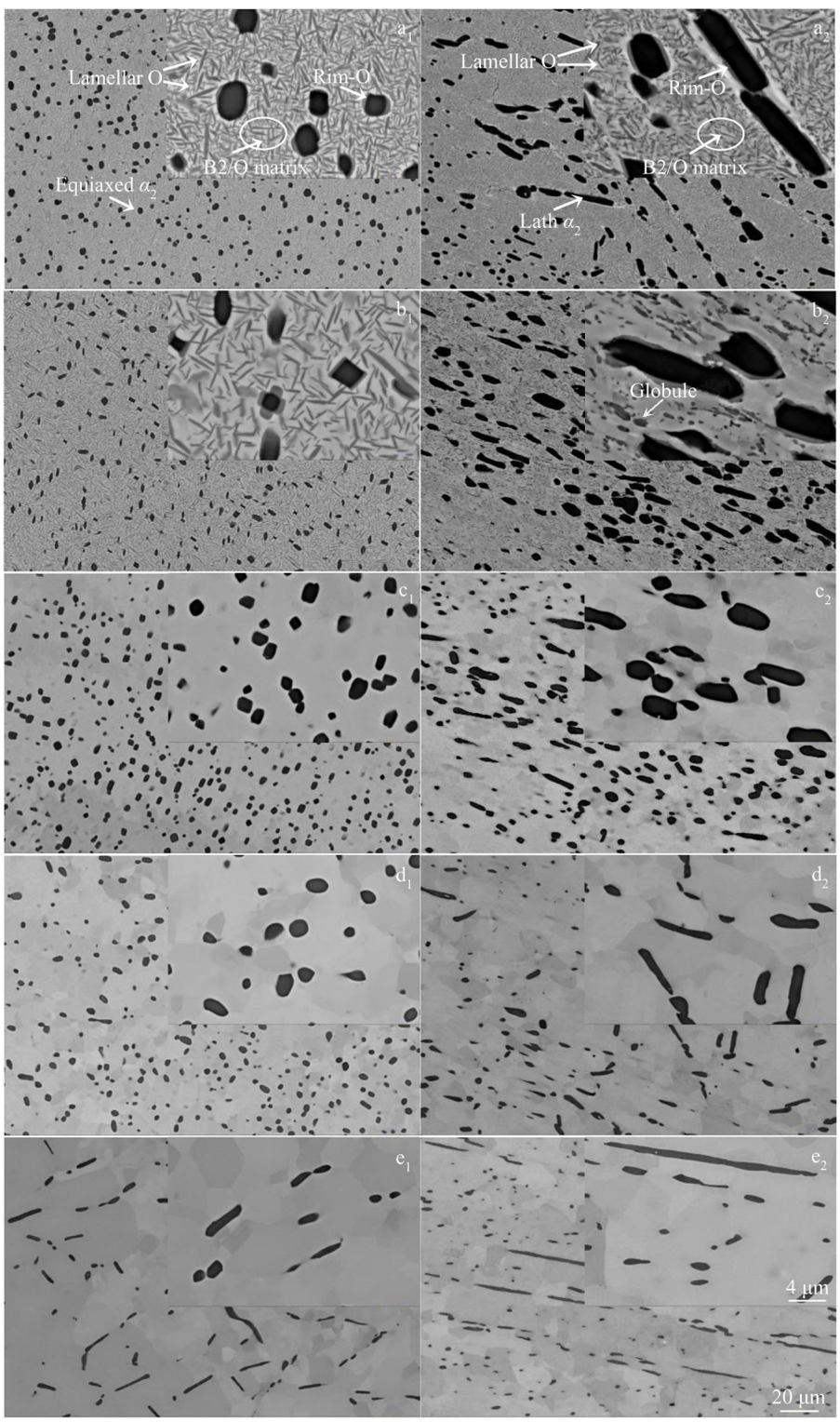

Fig.4 SEM microstructures of Ti-22Al-25Ti alloys before (a_1–e_1) and after (a_2–e_2) tension at different temperatures with strain rate of 1×10^{-3} s^{-1}: (a_1, a_2) 1203 K; (b_1, b_2) 1223 K; (c_1, c_2) 1243 K; (d_1, d_2) 1263 K; (e_1, e_2) 1283 K

changed from the slatted shape to equiaxed shape with increasing the temperature. During the hot deformation, the softening is generally related to the globularization. The material with the globule microstructure would have the ideal workability and stable flow[29].

The temperature of phase transition α_2+B2/β+O→α_2+B2 in Ti-22Al-25Nb alloy is about 1243 K. Combined with Fig. 3e, the low deformation temperature (1203–1243 K) of Ti-22Al-25Nb alloy results in the α_2+B2/β+O three-phase region, and the high deformation temperature (1243–1283 K) leads to the α_2+B2 two-phase region. For the three-phase and two-phase regions, their deformation activation energies are very different from the calculated ones of 845 165 and 412 779 J/mol, respectively. During the hot deformation, the higher apparent activation energy in the α_2+B2/β +O three-phase region at lower deformation temperature is related to the globularization of lamellar O microstructure[30]. In addition, with increasing the forming temperature, the apparent activation energy in the α_2+B2 two-phase region at higher deformation temperature is much lower than that in the three-phase region. As a result, the Ti-22Al-25Ti alloys are easier to deform at higher temperatures.

3 Conclusions

1) The peak stress is increased with increasing the strain rate and decreasing the temperature for Ti-22Al-25Ti alloys. The peak stress occurs at the strain of about 0.05, which is independent of strain rate and deformation temperature.

2) In the α_2+B2/β+O three-phase region (1203–1243 K) and α_2+B2 two-phase region (1243 – 1283 K) of Ti-22Al-25Nb alloys, their tensile deformation activation energies are different from the calculated ones of 845 165 and 412 779 J/mol, respectively.

3) The constitutive equations for the tensile deformation of Ti-22Al-25Nb alloys are established: at 1203 – 1243 K, $\dot{\varepsilon} = 8.377 \times 10^{32}[\sinh(0.009\,271\,1\sigma_p)]^{2.570}\exp(-845\,165/RT)$; at 1243 – 1283 K, $\dot{\varepsilon} = 5.834 \times 10^{14}[\sinh(0.009\,271\,1\sigma_p)]^{3.112} \times \exp(-412\,779/RT)$.

References

1 Banerjee D, Gogia A K, Nandi T K *et al. Acta Metallurgica*[J], 1988, 36(4): 871

2 Nandy T K, Banerjee D. *Intermetallics*[J], 2000, 8(9 – 11): 1269

3 Song H, Wang Z J, He X D. *Transactions of Nonferrous Metals Society of China*[J], 2013, 23(1): 32

4 Yang S J, Nam S W, Hagiwara M. *Intermetallics*[J], 2004, 12(3): 261

5 Boehlert C J. *Materials Science and Engineering A*[J], 2000, 279(1–2): 118

6 Boehlert C J, Miracle D B. *Metallurgical and Materials Transactions A*[J], 1999, 30: 2349

7 Cowen C J, Boehlert C J. *Intermetallics*[J], 2006, 14(4): 412

8 Zhang P H, Zeng W D, Jia R C *et al. Materials Science and Engineering A*[J], 2021, 803: 140 492

9 Sim K H, Wang G, Son R C *et al. Powder Technology*[J], 2017, 317: 133

10 Lin P, Tang T T, Chi C Z *et al. Rare Metal Materials and Engineering*[J], 2018, 47(2): 416

11 Wu Y, Wang D J, Fan R L *et al. Rare Metal Materials and Engineering*[J], 2020, 49(6): 1825

12 Zhang S W, Xi M Z, Liu R *et al. Materials Science and Engineering A*[J], 2022, 850: 143 520

13 Wang G F, Sui X C, Liu Q *et al. Materials Science and Engineering A*[J], 2021, 801: 140 392

14 Xue K M, Hu Y, Shi Y B *et al*. *Rare Metal Materials and Engineering*[J], 2019, 48(8): 2556

15 He Y S, Hu R, Luo W Z *et al*. *Rare Metal Materials and Engineering*[J], 2018, 47(11): 3460

16 Li Y J, Zhao Y, Wu A P *et al*. *Rare Metal Materials and Engineering*[J], 2017, 46(5): 1341

17 Zhan M, Du H F, Liu J *et al. Materials Science and Engineering A*[J], 2010, 527(12): 2864

18 Rokni M R, Zarei-Hanzaki A, Roostaei A A *et al. Materials & Design*[J], 2011, 32(10): 4955

19 Luo J, Li M Q, Ma D W. *Materials Science and Engineering A*[J], 2012, 532: 548

20 Li H Y, Li Y H, Wang X F *et al. Materials & Design*[J], 2013, 49: 493

21 Li H P, He L F, Zhao G Q *et al. Materials Science and Engineering A*[J], 2013, 580: 330

22 Li H Y, Wang X F, Wei D D *et al. Materials Science and Engineering A*[J], 2012, 536: 216

23 Richardson G J, Sellars C M, Tegart W J M. *Acta Metallurgica*[J], 1966, 14(10): 1225

24 Zeng Z P, Jonsson S, Zhang Y S. *Materials Science and Engineering A*[J], 2009, 505(1–2): 116

25 Lin P, He Z B, Yuan S J *et al. Materials Science and Engineering A*[J], 2012, 556: 617

26 Zhang M J, Li F G, Wang S Y *et al. Materials Science and Engineering A*[J], 2010, 527(24–25): 6771

27 Shi C, Mao W, Chen X G. *Materials Science and Engineering A*[J], 2013, 571: 83

28 Samantaray D, Mandal S, Bhaduri A K *et al. Transactions of the Indian Institute of Metals*[J], 2010, 63(6): 823

29 Seshacharyulu T, Medeiros S C, Morgan J T *et al. Materials Science and Engineering A*[J], 2000, 279(1–2): 289

30 Ma X, Zeng W D, Xu B *et al. Intermetallics*[J], 2012, 20(1): 1

Ti-22Al-25Nb合金板材高温拉伸变形行为的本构模型

鲁羽鹏[1]，孟令健[1]，殷宏亮[1]，林　鹏[1,2]

(1. 太原理工大学 材料科学与工程学院，山西 太原 030024)

(2. 哈尔滨工业大学 金属精密热加工国家级重点实验室，黑龙江 哈尔滨 150001)

摘　要：在1203~1283 K的温度范围内，以20 K的温度间隔对O相Ti-22Al-25Nb合金进行了等温单向拉伸试验，应变速率为2.5×10^{-4}、5.0×10^{-4}、1×10^{-3}、2×10^{-3}、4×10^{-3}、1×10^{-2}和5×10^{-2} s^{-1}，并对不同变形温度下的试样组织进行了表征。通过实验结果，确定了本构模型的材料常数；α_2+B2/β+O三相区（1203~1243 K）和α_2+B2两相区（1243~1283 K）的拉伸变形激活能分别为845 165和412 779 J/mol。构建了Arrhenius本构模型来描述Ti-22Al-25Nb合金在不同温度下的拉伸变形行为。

关键词：Ti_2AlNb；本构模型；微观组织；变形行为

作者简介：鲁羽鹏，男，1997年生，硕士，太原理工大学材料科学与工程学院，山西 太原 030024，E-mail：2948490550@qq.com